CHAPTER IV

RESULTS AND DISCUSSION

4.1 Basicity of 25,27-{2,2′-[2,2′-((2,5,8-triaza)nonyl)diphenoxy]diethyl}-*p-tert*-butylcalix[4]arene

The protonation constants of the 25,27-{2,2′-[2,2′-((2,5,8-triaza)nonyl) diphenoxy]diethyl}-*p-tert*-butylcalix[4]arene, **L** expressed in terms of logarithm of its values, at 25 °C in the methanolic solution of 5.0 x 10^{-2} M Et_4NClO_4 and 5.0 x 10^{-2} M $Bu_4NCF_3SO_3$, are shown in Table 4.1 and Table 4.2 respectively.

Table 4.1 Logarithm of the protonation constants of 25,27-{2,2′-[2,2′-((2,5,8-triaza)nonyl)diphenoxy]diethyl}-*p-tert*-butylcalix[4]arene **(L)** in the methanolic solution of 5.0 x 10^{-2} M Et_4NClO_4 at 25° C.

Protonation	log K
K_1 : $L + H^+ \rightleftharpoons LH^+$	11.50 ± 0.04
K_2 : $LH^+ + H^+ \rightleftharpoons LH_2^{2+}$	9.38 ± 0.09
K_3 : $LH_2^{2+} + H^+ \rightleftharpoons LH_3^{3+}$	3.22 ± 0.11

Table 4.2 Logarithm of the protonation constants of 25,27-{2,2′-[2,2′-((2,5,8-triaza)nonyl)diphenoxy]diethyl}-*p-tert*-butylcalix[4]arene (**L**) in the methanolic solution of 5.0 x 10^{-2} M $Bu_4NCF_3SO_3$ at 25° C.

Protonation	log K
K_1 : L + H^+ $\rightleftharpoons$ LH^+	10.45 ± 0.03
K_2 : LH^+ + H^+ $\rightleftharpoons$ LH_2^{2+}	8.32 ± 0.07
K_3 : LH_2^{2+} + H^+ $\rightleftharpoons$ LH_3^{3+}	2.74 ± 0.11

The titration curves of the 25,27-{2,2′-[2,2′-((2,5,8-triaza)nonyl)diphenoxy] diethyl}-*p-tert*-butylcalix[4]arene, **L** in the methanolic solution of 5.0 x 10^{-2} M Et_4NClO_4 and 5.0 x 10^{-2} M $Bu_4NCF_3SO_3$ at different initial concentrations shown in Figure 4.1 and Figure 4.2 respectively, indicate that the basicities of the ligand **L** are occurred at the higher pH. The plot between $\bar{p}$ and log [H^+] for the ligand **L** in the methanolic solution of 5.0 x 10^{-2} M Et_4NClO_4 and 5.0 x 10^{-2} M $Bu_4NCF_3SO_3$, shown in Figure 4.3 and 4.4 respectively, obviously indicate the average number of proton bound the ligand **L** of 2 within the range of log [H^+] of -4.8 to -7.8 and -4.0 to -7.0 respectively. The $\bar{p}$ of the ligand **L** (see Figure 4.3 and 4.4) approached 3 at the very high proton concentration indicate that at least three protonated species of the ligand **L** were formed.

According to the results in Table 4.1 and 4.2, order of magnitude of the first, second and third protonation constants of ligand **L** in the methanolic solution of 5.0 x 10^{-2} M Et_4NClO_4 and 5.0 x 10^{-2} M $Bu_4NCF_3SO_3$ are in the same sequence. From the results tabulated in Table 4.1 and 4.2, it shows that the magnitude of three protonation constants of the ligand **L** in the methanolic solution of 5.0 x 10^{-2} M $Bu_4NCF_3SO_3$ is lower than those in the methanolic solution of 5.0 x 10^{-2} M

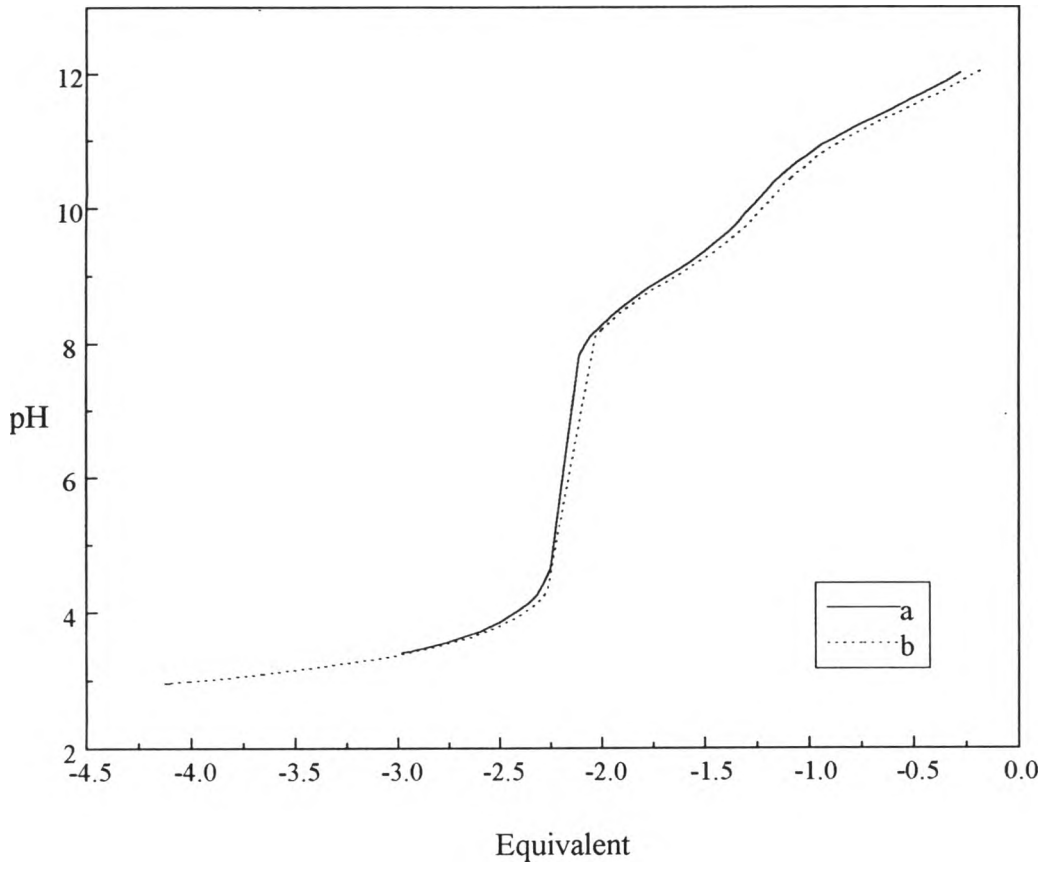

Figure 4.1 Potentiometric titration curves of the 25,27-{2,2′-[2,2′-((2,5.8-triaza) nonyl)diphenoxy]diethyl}-*p-tert*-butylcalix[4]arene **(L)** in the methanolic solution of 5.0 x 10^{-2} M Et_4NClO_4, based on the initial concentration ratio of the ligand **L** to proton of (a) 0.77 mM : 2.31 mM, and (b) 0.73 mM : 3.02 mM. Equivalent is defined as the ratio of ($n_{OH^-} - n_{acid}$) to n_{ligand}.

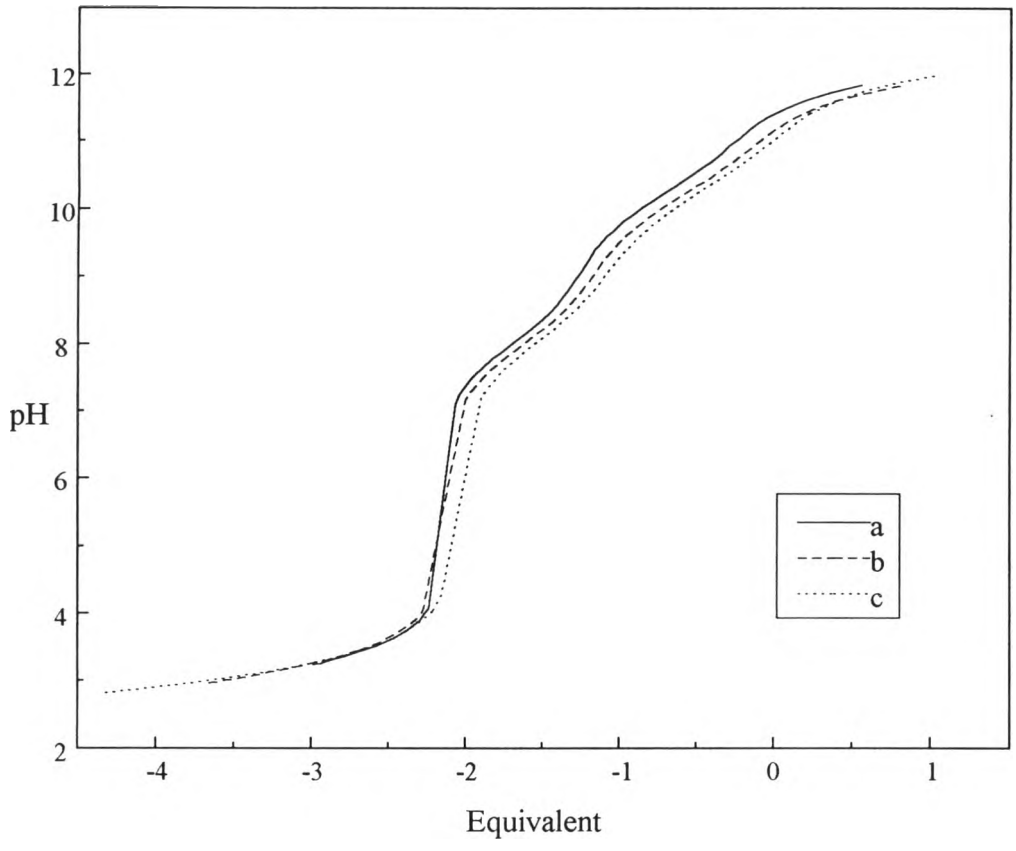

Figure 4.2 Potentiometric titration curves of the 25,27-{2,2′-[2,2′-((2,5.8-triaza) nonyl)diphenoxy]diethyl}-*p-tert*-butylcalix[4]arene **(L)** in the methanolic solution of 5.0 x 10^{-2} M $Bu_4NCF_3SO_3$, based on the initial concentration ratio of the ligand **L** to proton of (a) 0.83 mM : 2.49 mM, (b) 0.80 mM : 4.47 mM, and (c) 0.77 mM : 6.30 mM. Equivalent is defined as the ratio of ($n_{OH^-} - n_{acid}$) to n_{ligand}.

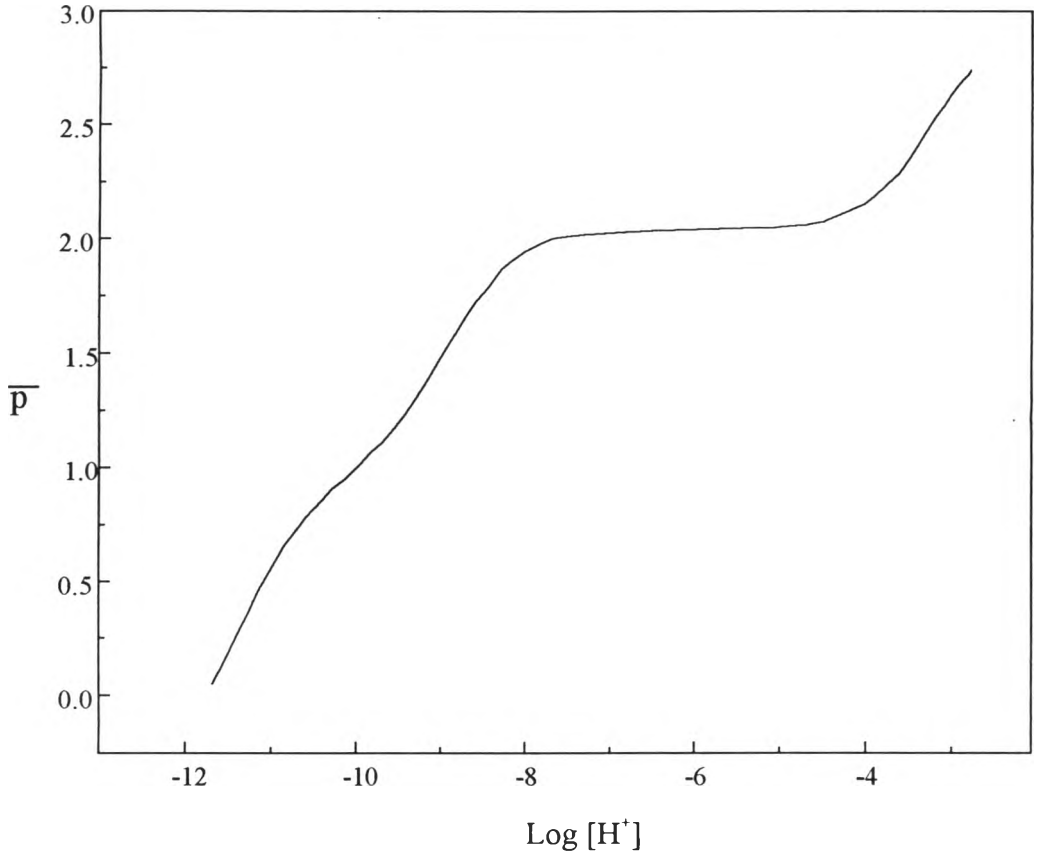

Figure 4.3 Plot between $\bar{p}$ and log [H^+] for the 25,27-{2,2′-[2,2′-((2,5.8-triaza) nonyl)diphenoxy]diethyl}-*p-tert*-butylcalix[4]arene in the methanolic solution of 5.0 x 10^{-2} M Et_4NClO_4, based on the initial concentration ratio of the ligand **L** to proton of 0.67 mM : 3.57 mM.

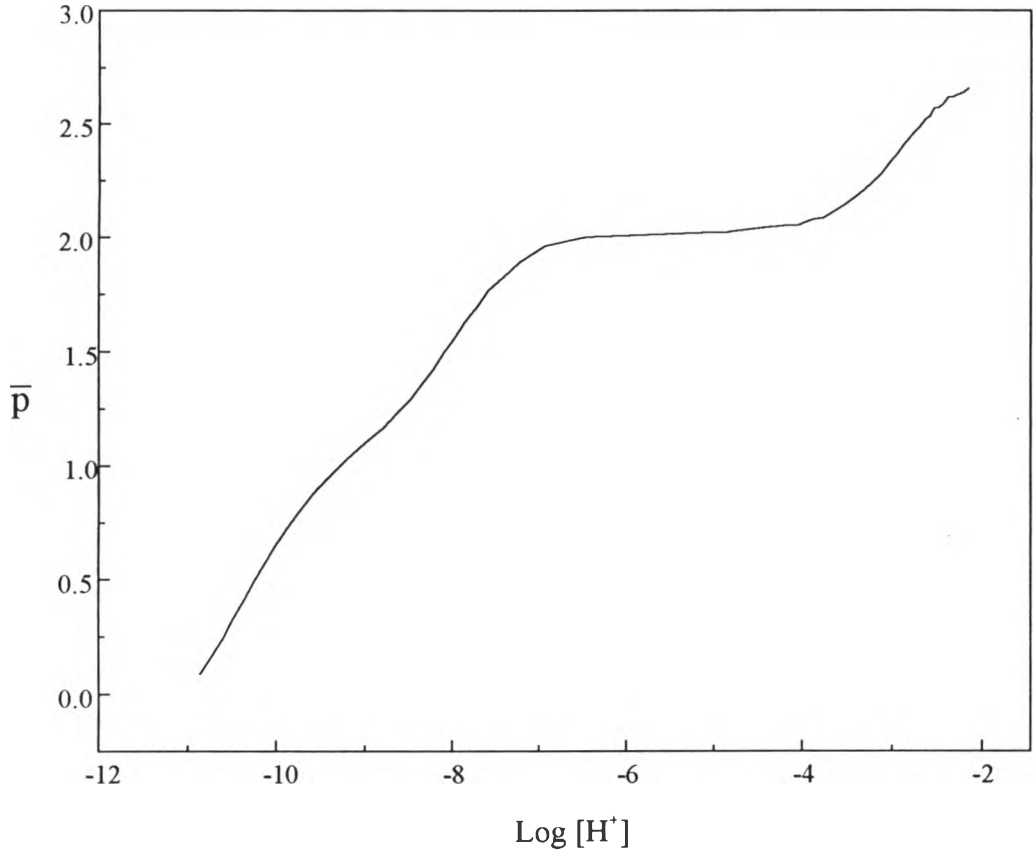

Figure 4.4 Plot between $\bar{p}$ and log [H^+] for the 25,27-{2,2′-[2,2′-((2,5.8-triaza) nonyl)diphenoxy]diethyl}-*p-tert*-butylcalix[4]arene in the methanolic solution of 5.0 x 10^{-2} M $Bu_4NCF_3SO_3$, based on the initial concentration ratio of the ligand **L** to proton of 0.77 mM : 6.30 mM.

Et_4NClO_4. Therefore, the $Bu_4NCF_3SO_3$ can be used as a new inert background electrolyte in the methanolic solution. Many tetraalkylammonium salts of perfluoroalkanesulfonates could be expected to be inert background electrolyte for determination of the equilibrium constants in the methanolic solution because the acids of perfluoroalkanesulfonates are all strong acids[28].

The basicity of the similar structure of 25,27-{2,2′-[2,2′-((2,5,8-triaza)nonyl) diphenoxy]diethyl}-*p-tert*-butylcalix[4]arene such as 1,12,15-triaza-3,4 : 9,10-dibenzo-5,8-dioxacycloheptadecane (see Figure 4.5) was studied in the methanolic solution of 1.0 x 10^{-1} M Me_4NCl. The logarithm of the first, second and third protonation constants of 1,12,15-triaza-3,4 : 9,10-dibenzo-5,8-dioxacycloheptadecane in the methanolic solution of 1.0 x 10^{-1} M Me_4NCl of 9.47 (± 0.05), 8.27 (± 0.05) and 2.35 (± 0.2) respectively, were found [1]. The order of magnitude of the first, second and third protonation constants according to the 25,27-{2,2′-[2,2′-((2,5,8-triaza)nonyl) diphenoxy]diethyl}-*p-tert*-butylcalix[4]arene is in the same sequence of the protonation constants according to the1,12,15-triaza-3,4:9,10-dibenzo-5,8-dioxacycloheptadecane.

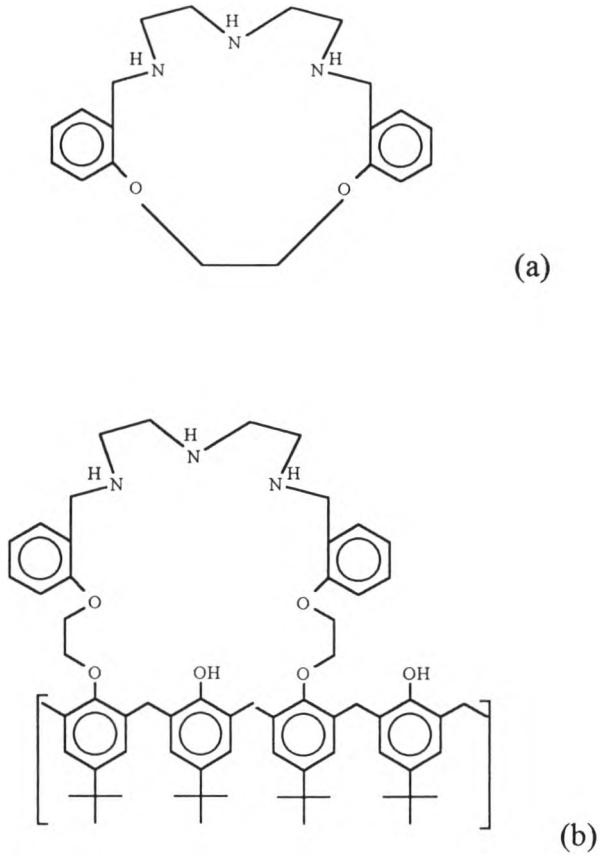

Figure 4.5 Structural comparison between (a) 1,12,15-triaza-3,4 : 9,10-dibenzo-5,8-dioxacycloheptadecane and (b) 25,27-{2,2′-[2,2′-((2,5,8-triaza)nonyl)diphenoxy] diethyl}-*p-tert*-butylcalix[4]arene.

The species distribution of 25,27-{2,2′-[2,2′-((2,5,8-triaza)nonyl)diphenoxy] diethyl}-*p-tert*-butylcalix[4]arene in the methanolic solution of 5.0 x 10^{-2} M Et_4NClO_4 at 25°C, (Figure 4.6). The LH_3^{3+} species is steeply decreased from over 60 mole percent at pH 3.0 to less than 5 % at pH higher than 5.0. The LH_2^{2+} exists over 90 % within the pH range of 5.0 to 7.5 and over 30 % within the pH range of 3.0 to 9.0 . At neutral pH 8.3, the mole percent of protonated species, the LH_2^{2+} and LH^+ are about 80 % and 20 % respectively. The maximum population of the LH^+ is located at pH

10.0. The L species exists at pH higher than 9.0 and its population over 90 % is found at pH above 12.

The species distribution of 25,27-{2,2′-[2,2′-((2,5,8-triaza)nonyl)diphenoxy] diethyl}-*p-tert*-butylcalix[4]arene in the methanolic solution of 5.0 x 10^{-2} M $Bu_4NCF_3SO_3$ at 25°C (Figure 4.7), is quite similar to the system in the methanolic solution of 5.0 x 10^{-2} M Et_4NClO_4. The LH_3^{3+} species is steeply decreased from about 70 % mole at pH 2.8 to less than 5% at pH higher than 4.5. Over 90 % of the LH_2^{2+} exists within the pH range of 4.0 to 7.0. At pH 7.0, only the LH_2^{2+} species exists in the solution. At the neutral, at pH = 8.3, the mole percent of protonated species, the LH_2^{2+} and LH^+ are over 38 % and 60 % respectively. The LH^+ species is absent at the pH below 6.5 but dominant species at the pH about 9. The free ligand species, L, at exists the pH higher than 8.0 and its population is increased as the pH function.

The species distribution of 25,27-{2,2′-[2,2′-((2,5,8-triaza)nonyl)diphenoxy] diethyl}-*p-tert*-butylcalix[4]arene in the methanolic solution of 5.0 x 10^{-2} M $Bu_4NCF_3SO_3$ and 5.0 x 10^{-2} M Et_4NClO_4 at 25 °C computed from its protonation constants and titrating data, are shown in Figure 4.6 and 4.7 respectively. Species domination of the ligand **L** in both electrolyte depending on the pH of the methanolic solution in the sequence of $LH_3^{3+} < LH_2^{2+} < LH^+ < L$ at increasing pH. At 25 °C, over 50% of LH_2^{2+} in methanolic solution of 5.0 x 10^{-2} M $Bu_4NCF_3SO_3$ and 5.0 x 10^{-2} M Et_4NClO_4 located as the major species within the pH range of 3-8 and 3.5-9, respectively. In both electrolyte solutions, the complete protonated species, LH_3^{3+} occur in the pH below 7. Maximum population of LH^+ in the methanolic solution of 5.0 x 10^{-2} M $Bu_4NCF_3SO_3$ and 5x10^{-2} M Et_4NClO_4 about 80 % are located at pH 9.2 and 10, respectively. Deprotonated form of L in both electrolyte solutions are found at the pH above 9.

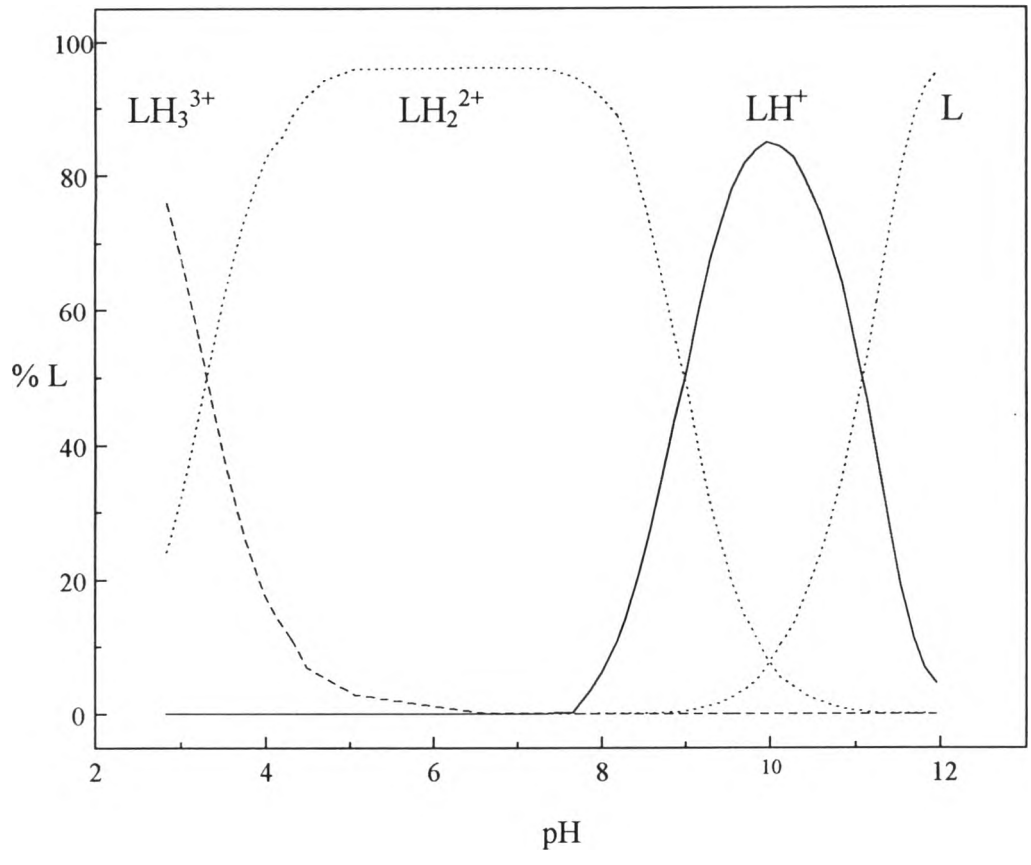

Figure 4.6 Species distribution of the 25,27-{2,2′-[2,2′-((2,5,8-triaza)nonyl) diphenoxy]diethyl}-*p-tert*-butylcalix[4]arene in the methanolic solution of 5.0 x 10^{-2} M Et_4NClO_4 at 25 °C, C_L = 0.67 mM.

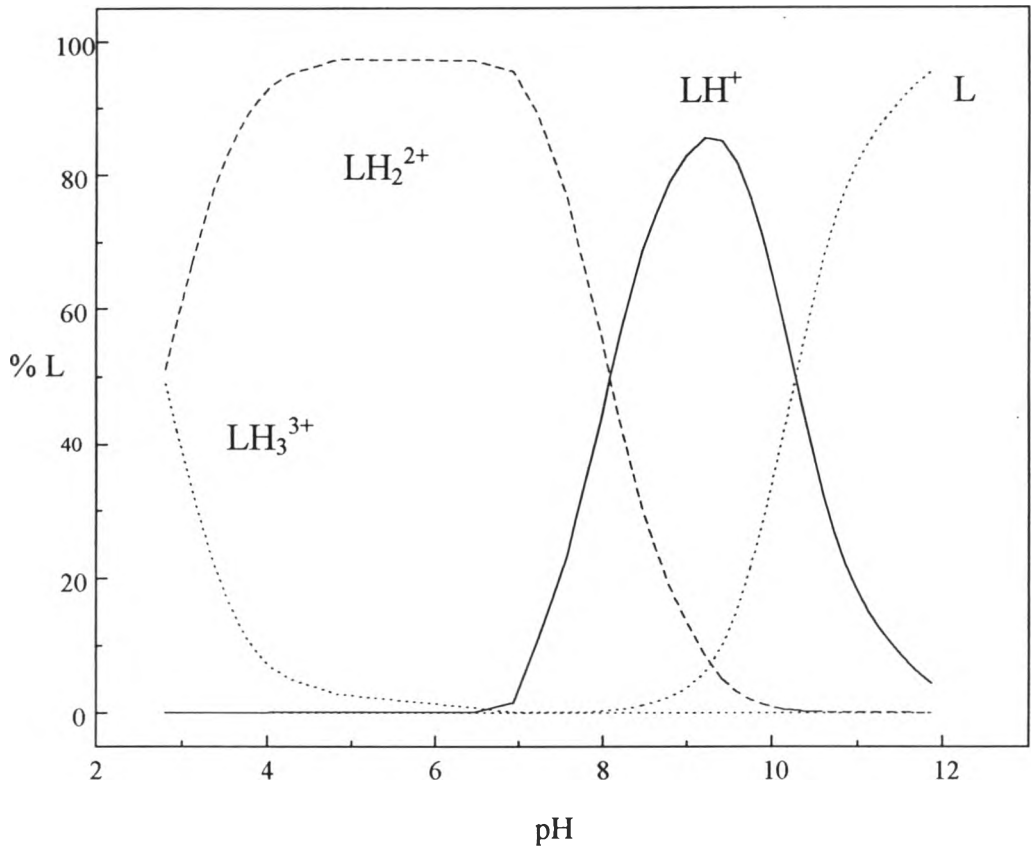

Figure 4.7 Species distribution of the 25,27-{2,2′-[2,2′-((2,5,8-triaza)nonyl) diphenoxy]diethyl}-*p-tert*-butylcalix[4]arene in the methanolic solution of 5.0 x 10^{-2} M $Bu_4NCF_3SO_3$ at 25 °C, C_L = 0.77 mM.

4.2 Complexation of 25,27-{2,2′-[2,2′-((2,5,8-triaza)nonyl)diphenoxy]diethyl}-*p-tert*-butylcalix[4]arene with Divalent Transition Metal Ions

Stability constants of the complexes of the ligand **L** in terms of logarithm shown in Table 4.3.

Table 4.3 Logarithm of the stability constants (log β) of the 25,27-{2,2′-[2,2′-((2,5.8-triaza)nonyl)diphenoxy]diethyl}-*p-tert*-butylcalix[4]arene complexes with divalent transition metal ions in methanolic solution of 5.0×10^{-2} M $Bu_4NCF_3SO_3$ at $25 \pm 0.1^{\circ}C$.

M^{2+}	log β		
	ML^{2+}	$ML(CH_3O)^{+}$	M_2L^{4+}
Co^{2+}	7.57 ± 0.03	-	-
Ni^{2+}	9.06 ± 0.04	-	-
Cu^{2+}	15.27 ± 0.04	6.01 ± 0.08	-
Zn^{2+}	7.17 ± 0.09	-	12.38 ± 0.08

The titration curves of the complexes between the ligand **L** with the divalent transition metal ions (Co^{2+}, Ni^{2+}, Cu^{2+} and Zn^{2+}) in the methanolic solution of 5.0×10^{-2} M $Bu_4NCF_3SO_3$ at various initial concentrations of metal and ligand **L**, shown in Figure 4.8, 4.9, 4.10 and 4.11 respectively indicate that the complexation of reacting species for each titration should occurred at the higher hydroxide equivalent. The equilibria for Co^{2+}, Cu^{2+} and Zn^{2+} were established quickly while for Ni^{2+} longer equilibration times were required.

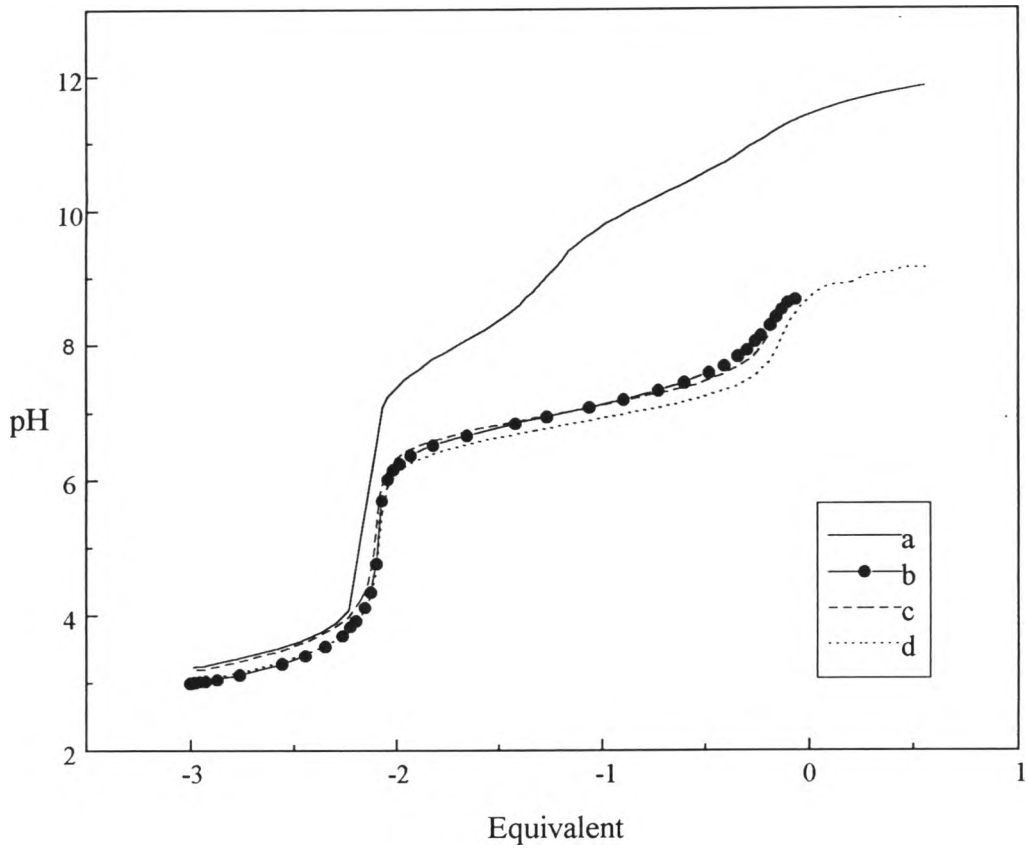

Figure 4.8 Potentiometric titration curves of the 25,27-{2,2′-[2,2′-((2,5.8-triaza) nonyl)diphenoxy]diethyl}-*p-tert*-butylcalix[4]arene in the methanolic solution of 5.0 x 10^{-2} M $Bu_4NCF_3SO_3$ (a) at C_L = 0.83 mM and its complex with Co^{2+}, based on the initial concentration ratio of the ligand **L** to Co^{2+} of (b) 0.83 mM : 0.84 mM, (c) 0.80 mM : 1.21 mM, and (d) 0.83 mM : 1.67 mM. Equivalent is defined as the ratio of ($n_{OH^-} - n_{acid}$) to n_{ligand}.

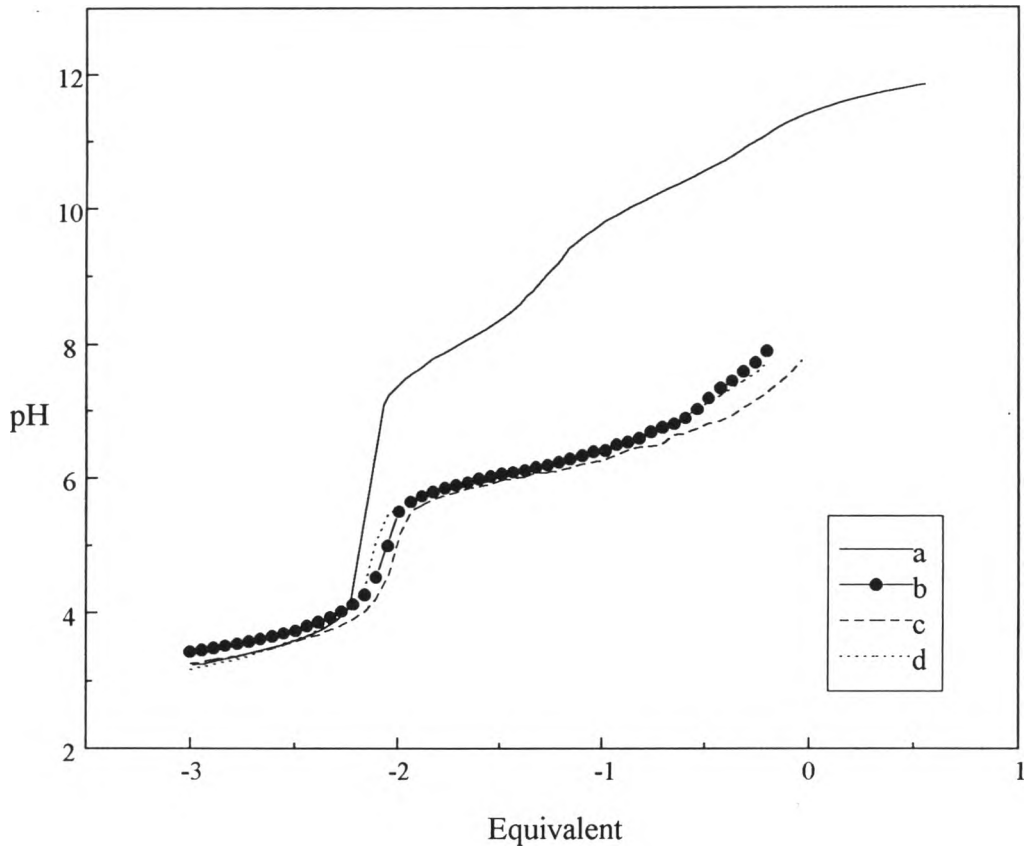

Figure 4.9 Potentiometric titration curves of the 25,27-{2,2′-[2,2′-((2,5.8-triaza) nonyl)diphenoxy]diethyl}-*p-tert*-butylcalix[4]arene in the methanolic solution of 5.0 x 10^{-2} M $Bu_4NCF_3SO_3$ (a) at C_L = 0.83 mM and its complex with Ni^{2+}, based on the initial concentration ratio of the ligand **L** to Ni^{2+} of (b) 0.83 mM : 0.84 mM, (c) 0.80 mM : 1.20 mM, and (d) 0.83 mM : 1.67 mM. Equivalent is defined as the ratio of $(n_{OH^-} - n_{acid})$ to n_{ligand}.

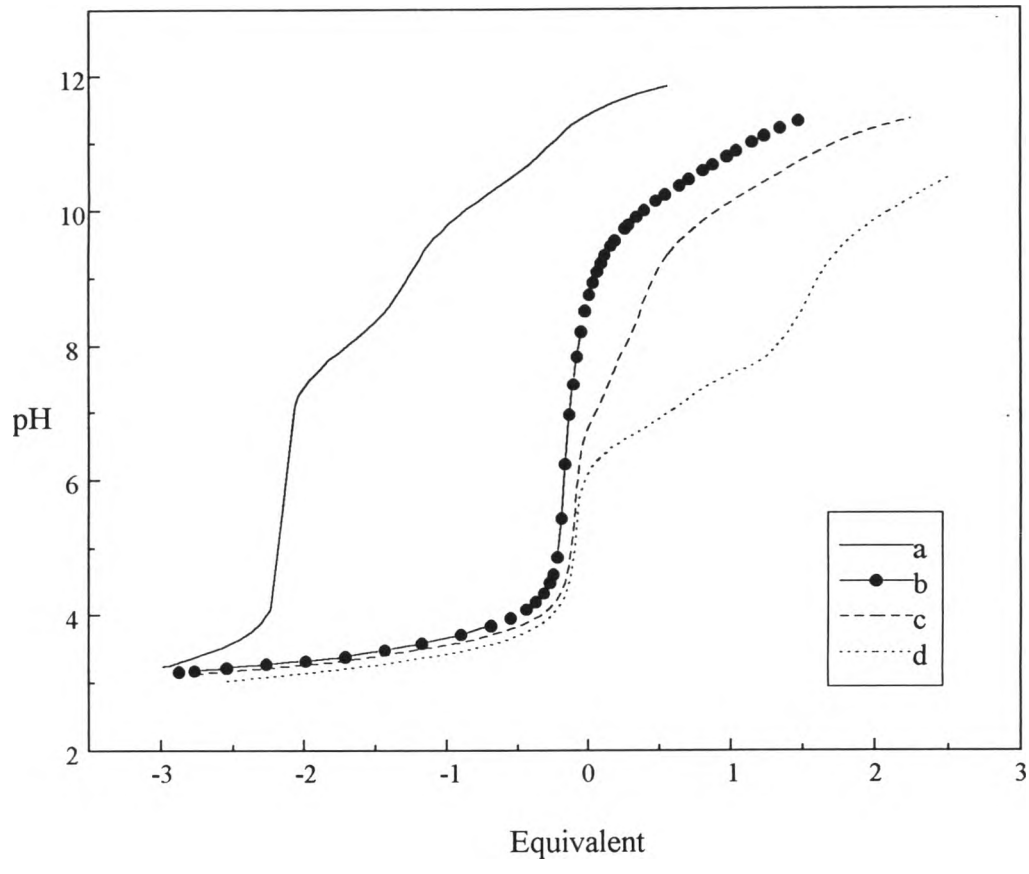

Figure 4.10 Potentiometric titration curves of the 25,27-{2,2′-[2,2′-((2,5.8-triaza) nonyl)diphenoxy]diethyl}-*p-tert*-butylcalix[4]arene in the methanolic solution of 5.0×10^{-2} M $Bu_4NCF_3SO_3$ (a) at C_L = 0.83 mM and its complex with Cu^{2+}, based on the initial concentration ratio of the ligand **L** to Cu^{2+} of (b) 0.83 mM : 0.84 mM, (c) 0.81 mM : 1.06 mM, and (d) 0.83 mM : 1.68 mM. Equivalent is defined as the ratio of $(n_{OH^-} - n_{acid})$ to n_{ligand}.

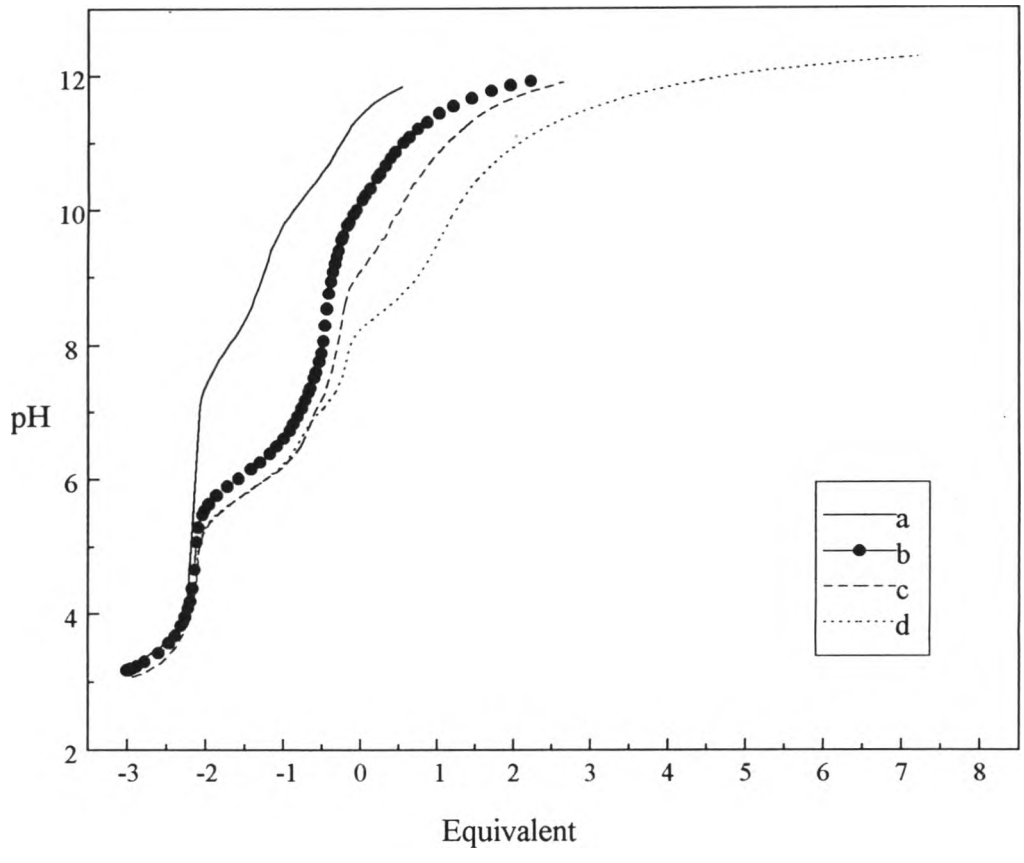

Figure 4.11 Potentiometric titration curves of the 25,27-{2,2′-[2,2′-((2,5.8-triaza) nonyl)diphenoxy]diethyl}-*p-tert*-butylcalix[4]arene in the methanolic solution of 5.0 x 10^{-2} M $Bu_4NCF_3SO_3$ (a) at C_L = 0.83 mM and its complex with Zn^{2+}, based on the initial concentration ratio of the ligand **L** to Zn^{2+} of (b) 0.83 mM : 0.83 mM, (c) 0.80 mM : 1.20 mM, and (d) 0.84 mM : 1.67 mM. Equivalent is defined as the ratio of $(n_{OH^-} - n_{acid})$ to n_{ligand}.

The complex formation function, $\bar{n}$ of the 25,27-{2,2′-[2,2′-((2,5,8-triaza) nonyl)diphenoxy]diethyl}-*p-tert*-butylcalix[4]arene complexes with Co^{2+}, Ni^{2+}, Cu^{2+} and Zn^{2+} versus the log [L] are shown in Figure 4.12, 4.13, 4.14 and 4.15 respectively. The $\bar{n}$ of the 25,27-{2,2'-[2,2'-((2,5,8-triaza)nonyl)diphenoxy]diethyl}-*p-tert*-butylcalix[4]arene complexes with Co^{2+} and Ni^{2+}, approached to the unity at the higher concentration of the ligand **L** with the steep slope of $\bar{n}$ and log [L], confirm the existing of the single species of ML^{2+}. The plot between $\bar{n}$ and log [L] for the copper (II) complex with 25,27-{2,2'-[2,2'-((2,5,8-triaza)nonyl)diphenoxy]diethyl}-*p-tert*-butylcalix[4]arene (Figure 4.14) indicate that the existing complex(es) is (are) the ligand to metal ratio of 1 : 1. The complex formation function of zinc(II) complex with 25,27-{2,2′-[2,2′-((2,5,8-triaza)nonyl)diphenoxy]diethyl}-*p-tert*-butylcalix[4]arene shown in the Figure 4.15 indicates that at least species of the ligand **L** to Zn^{2+} ratio of 1 : 1 has been formed with the existing of other complex species.

The protonation equilibria concerned with the 25,27-{2,2′-[2,2′-((2,5,8-triaza) nonyl)diphenoxy]diethyl}-*p-tert*-butylcalix[4]arene (**L**) and its complexes with M^{2+} metal ions are shown below.

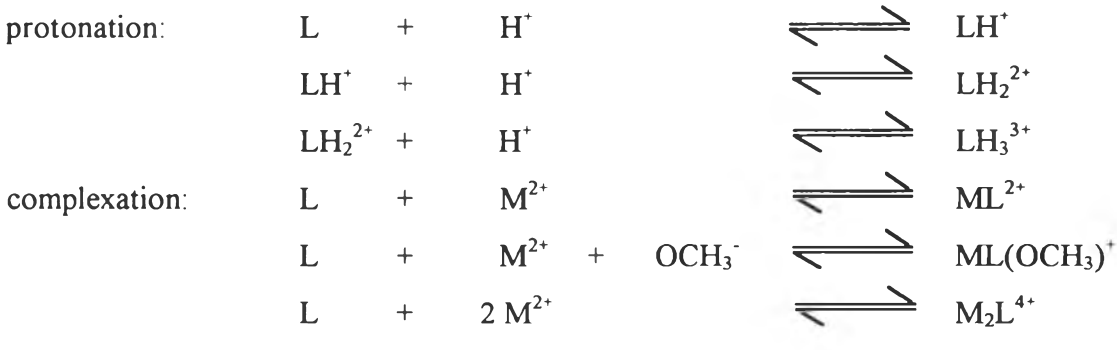

The species distribution curves of the complexes of 25,27-{2,2′-[2,2′-((2,5,8-triaza)nonyl)diphenoxy]diethyl}-*p-tert*-butylcalix[4]arene with Co^{2+}, Ni^{2+}, Cu^{2+}, and Zn^{2+} in the methanolic solution of 5.0×10^{-2} M $Bu_4NCF_3SO_3$ at 25 °C computed from their stability constants and titrating data, are shown in Figure 4.16 , 4.17, 4.18 and 4.19 respectively.

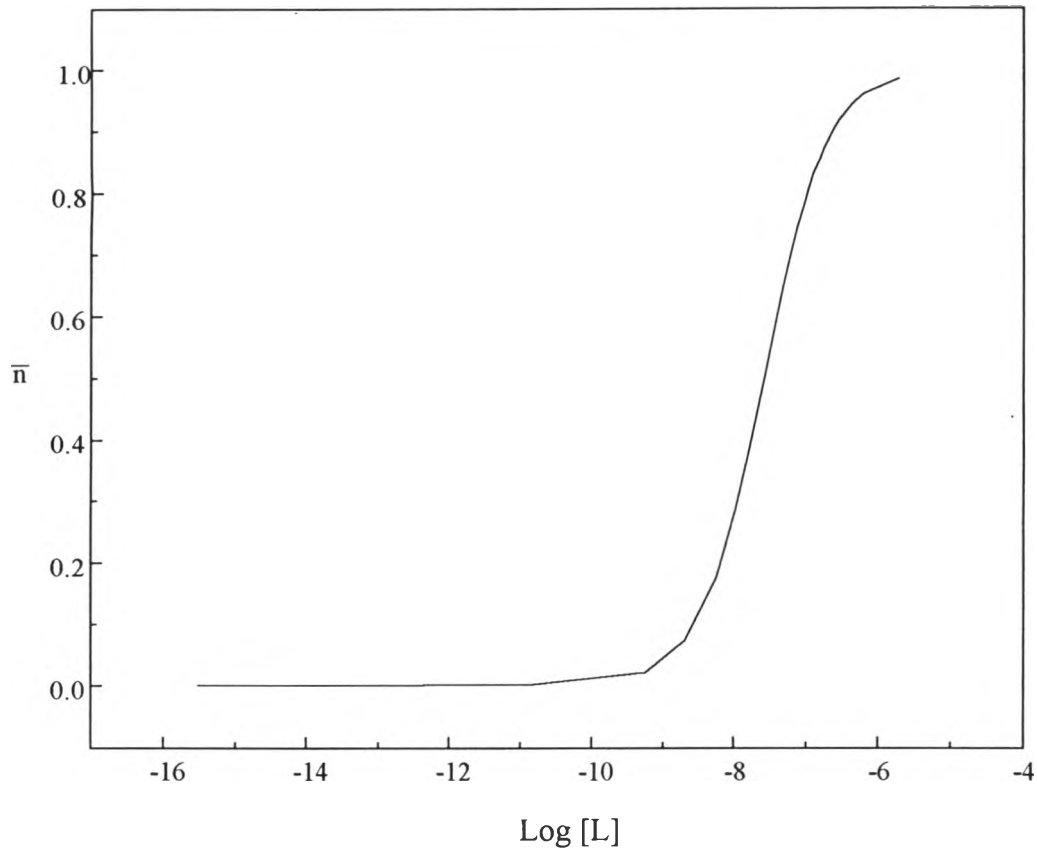

Figure 4.12 Plot between $\bar{n}$ and log [L] for the cobalt (II) complex with 25,27-{2,2′-[2,2′-((2,5.8-triaza)nonyl)diphenoxy]diethyl}-*p-tert*-butylcalix[4]arene in the methanolic solution of 5.0 x 10^{-2} M $Bu_4NCF_3SO_3$, based on the initial concentration ratio of the ligand **L** to Co^{2+} 0.83 mM : 0.84 mM.

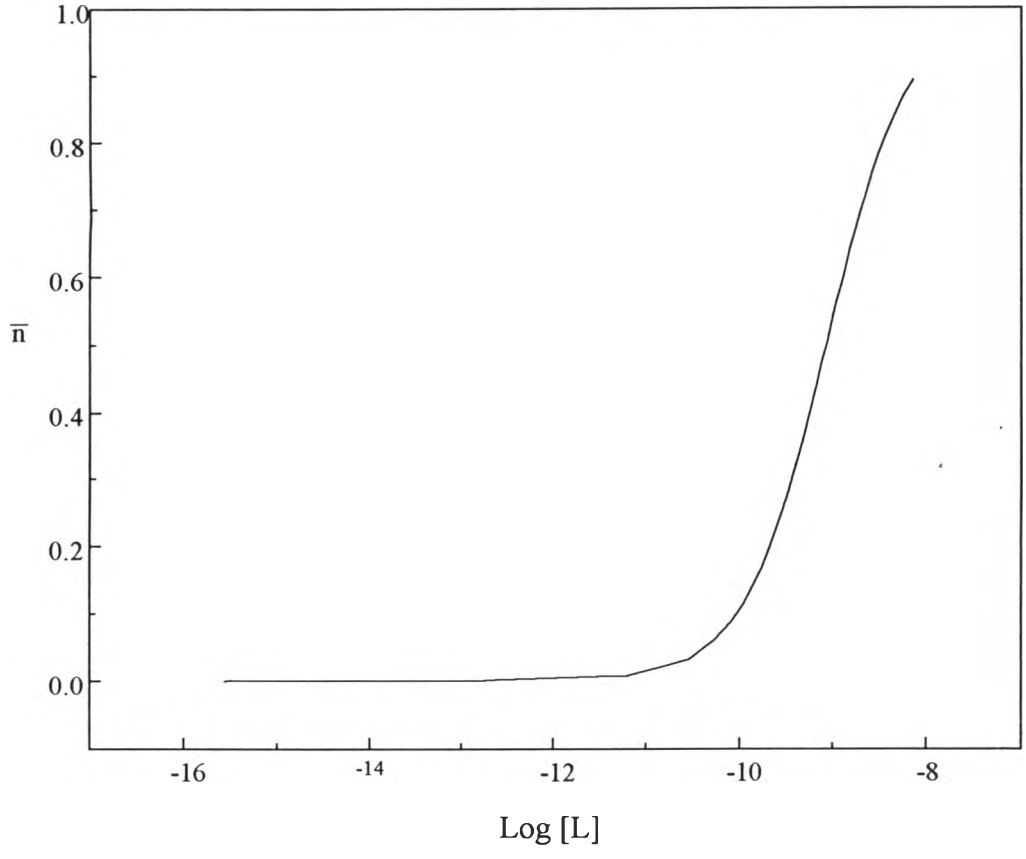

Figure 4.13 Plot between $\bar{n}$ and log [L] for the nickel (II) complex with 25,27-{2,2′-[2,2′-((2,5.8-triaza)nonyl)diphenoxy]diethyl}-*p-tert*-butylcalix[4]arene in the methanolic solution of 5.0 x 10^{-2} M $Bu_4NCF_3SO_3$, based on the initial concentration ratio of the ligand **L** to Ni^{2+} 0.83 mM : 0.84 mM.

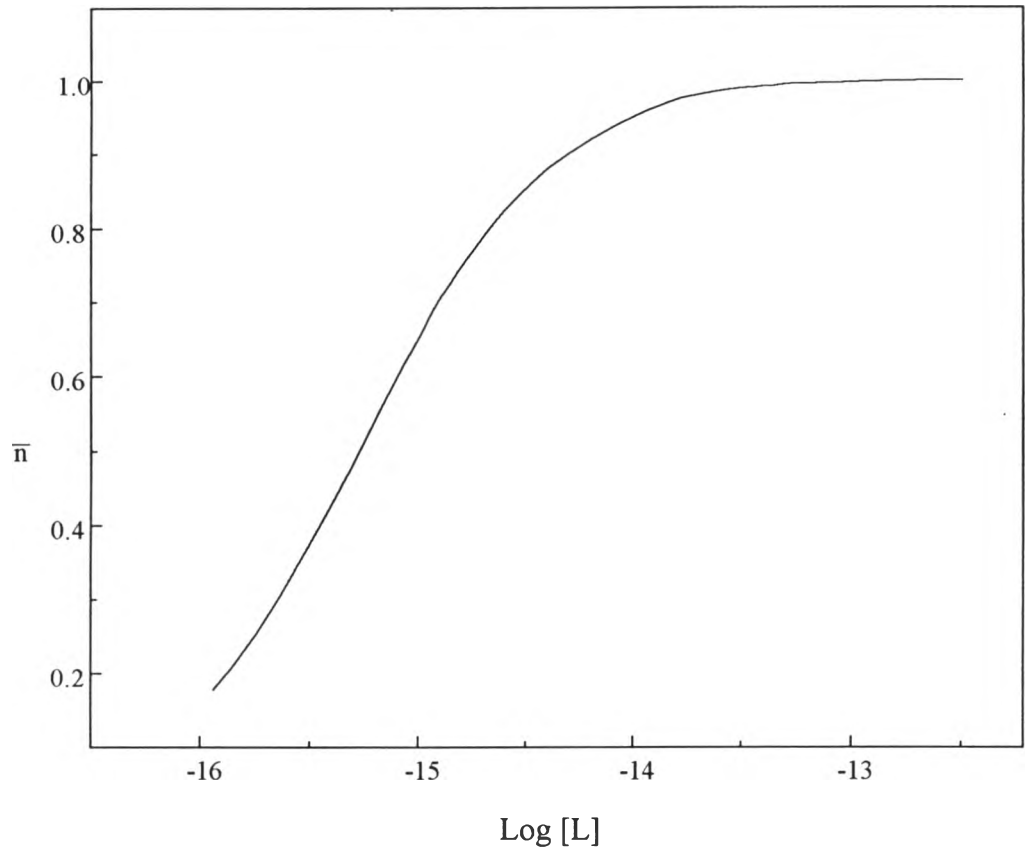

Figure 4.14 Plot between $\bar{n}$ and log [L] for the copper (II) complex with 25,27-{2,2′-[2,2′-((2,5.8-triaza)nonyl)diphenoxy]diethyl}-*p-tert*-butylcalix[4]arene in the methanolic solution of 5.0 x 10^{-2} M $Bu_4NCF_3SO_3$, based on the initial concentration ratio of the ligand **L** to Cu^{2+} 0.81 mM : 1.06 mM.

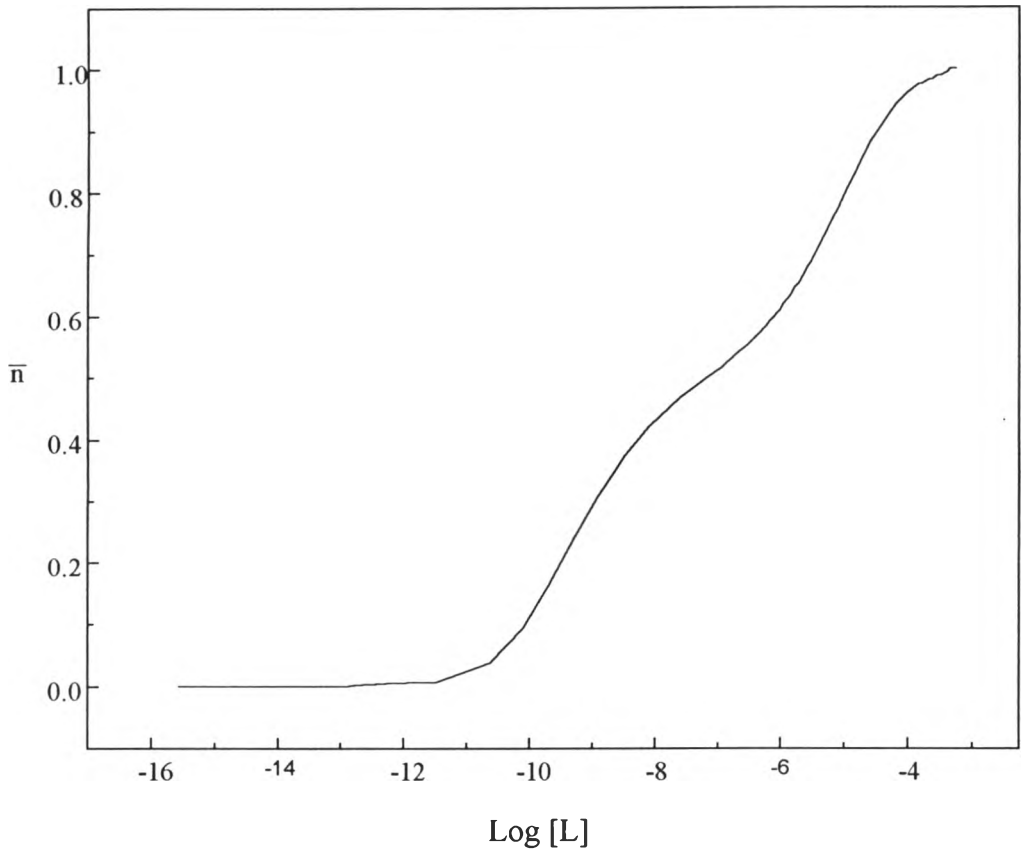

Figure 4.15 Plot between $\bar{n}$ and log [L] for the zinc (II) complex with 25,27-{2,2′-[2,2′-((2,5.8-triaza)nonyl)diphenoxy]diethyl}-*p-tert*-butylcalix[4]arene in the methanolic solution of 5.0 x 10^{-2} M $Bu_4NCF_3SO_3$, based on the initial concentration ratio of the ligand **L** to Zn^{2+} 0.84 mM : 0.83 mM.

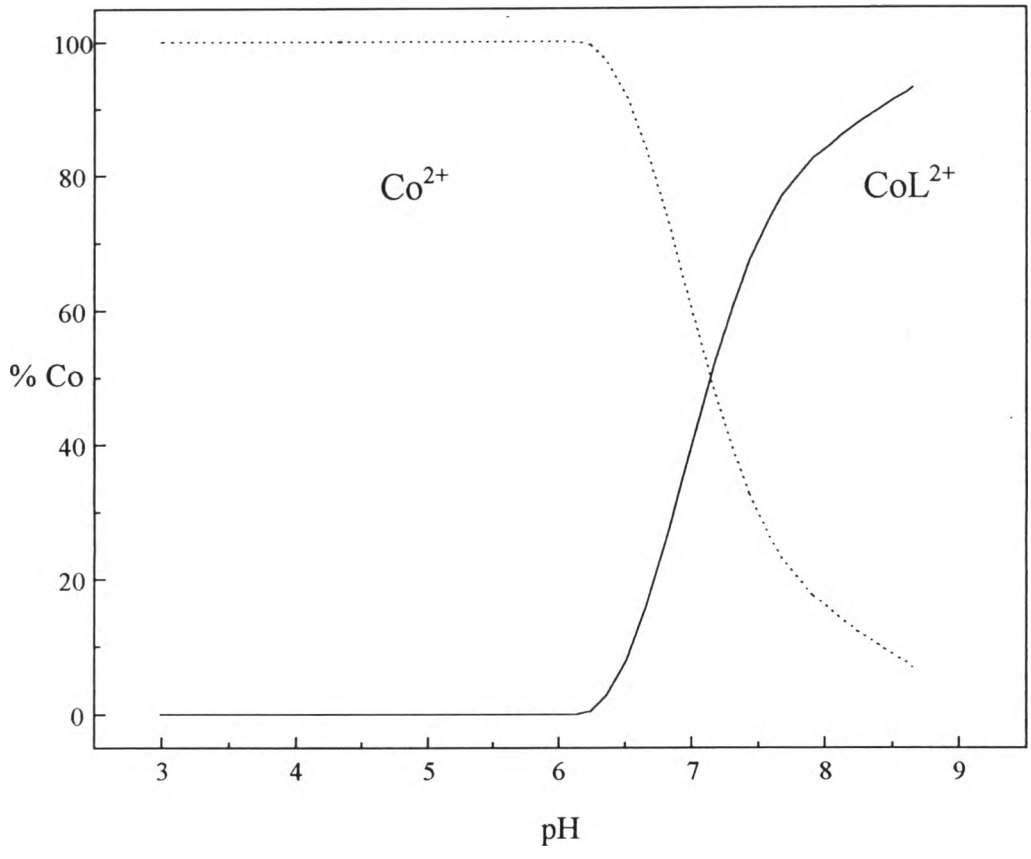

Figure 4.16 Species distribution of the cobalt (II) complex in the methanolic solution of 5.0 x 10^{-2} M $Bu_4NCF_3SO_3$ at 25° C, in the presence of the Co^{2+} and the 25,27-{2,2′-[2,2′-((2,5,8-triaza)nonyl)diphenoxy]diethyl}-*p*-*tert*-butylcalix[4]arene by the ratio of 0.84 mM to 0.83 mM.

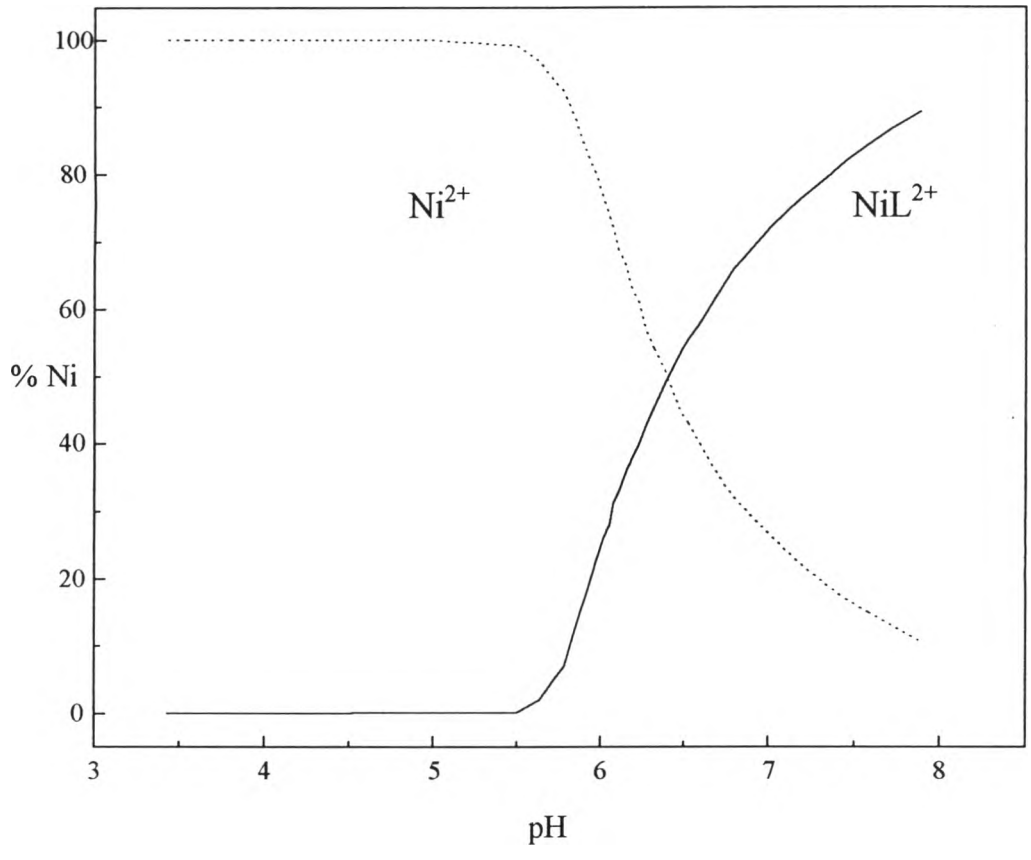

Figure 4.17 Species distribution of the nickel (II) complex in the methanolic solution of 5.0 x 10^{-2} M $Bu_4NCF_3SO_3$ at 25° C, in the presence of the Ni^{2+} and the 25,27-{2,2′-[2,2′-((2,5,8-triaza)nonyl)diphenoxy]diethyl}-*p-tert*-butylcalix[4]arene by the ratio of 0.84 mM to 0.83 mM.

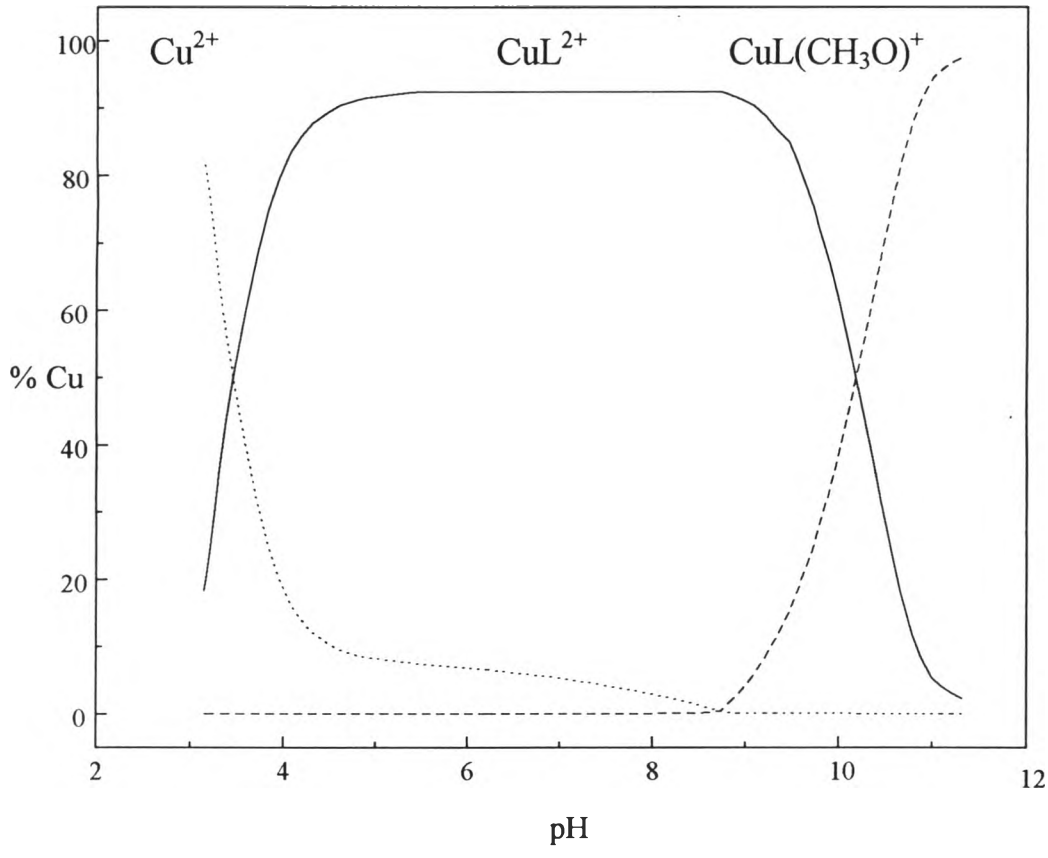

Figure 4.18 Species distribution of the copper (II) complex in the methanolic solution of 5.0 x 10^{-2} M $Bu_4NCF_3SO_3$ at 25° C, in the presence of the Cu^{2+} and the 25,27-{2,2′-[2,2′-((2,5,8-triaza)nonyl)diphenoxy]diethyl}-*p*-*tert*-butylcalix[4]arene by the ratio of 1.06 mM to 0.81 mM.

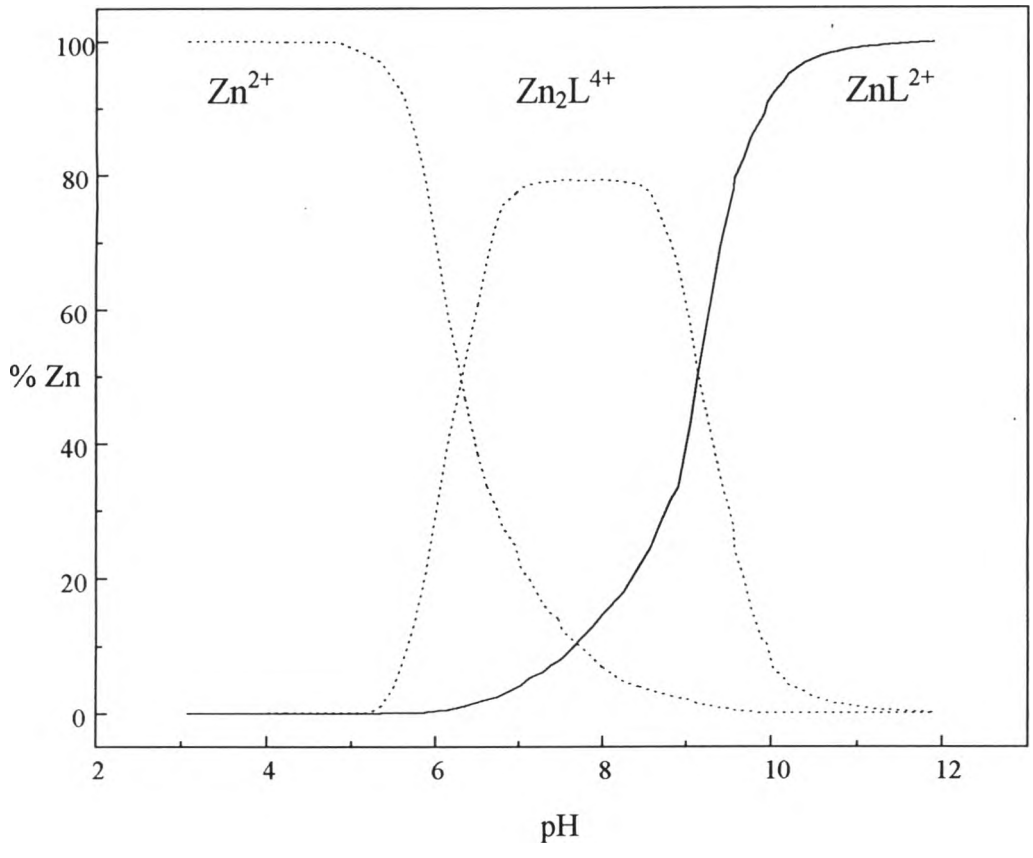

Figure 4.19 Species distribution of the zinc (II) complex in the methanolic solution of 5.0 x 10^{-2} M $Bu_4NCF_3SO_3$ at 25° C, in the presence of the Zn^{2+} and the 25,27-{2,2′-[2,2′-((2,5,8-triaza)nonyl)diphenoxy]diethyl}-*p-tert*-butylcalix[4]arene by the ratio of 0.83 mM to 0.84 mM.

The complexes of 25,27-{2,2′-[2,2′-((2,5,8-triaza)nonyl)diphenoxy]diethyl}-*p*-*tert*-butylcalix[4]arene with Co^{2+} and Ni^{2+}, only the ML^{2+} species is able to be formed. Over 50% of CoL^{2+} and NiL^{2+} are located at the pH over 7.5 and 6.5, respectively. The existing species of the complexes between 25,27-{2,2′-[2,2′-((2,5,8-triaza)nonyl) diphenoxy]diethyl}-*p*-*tert*-butylcalix[4]arene with Cu^{2+} are the form of CuL^{2+} and $CuL(CH_3O)^+$. CuL^{2+} is a major species that exists within the wide pH range of 4 to 10. At pH above 9, CuL^{2+} was methanolated by CH_3O^- to be a form of $CuL(CH_3O)^+$. Complexation between 25,27-{2,2′-[2,2′-((2,5,8-triaza)nonyl)diphenoxy]diethyl}-*p*-*tert*-butylcalix[4]arene with Zn^{2+} , results the species Zn_2L^{4+} and ZnL^{2+} in the methanolic solution at pH above 5.5. Zn_2L^{4+} can survive within the pH range of 6 to 10 and ZnL^{2+} is formed at pH above 6 and over 80% of its population appear at pH above 10.

According to the result in Table 4.3, the ML^{2+} species was found in every complexation of the divalent metal ions of the first transition series (Co^{2+}, Ni^{2+}, Cu^{2+} and Zn^{2+}) with the ligand **L**. Order magnitude of the stability constants for the formation of analogous complexes ML^{2+} are in the following order of the metal ions: $Co^{2+} < Ni^{2+} < Cu^{2+} > Zn^{2+}$ as shown in Figure 4.20 which correspond the expected Irving-Williams order[29]. Consideration of the stability constants for ML^{2+} species, the 25,27-{2,2′-[2,2′-((2,5,8-triaza)nonyl)diphenoxy]diethyl}-*p*-*tert*-butylcalix[4]arene, **L** has the most selectivity for metal ions as $Cu^{2+} >> Ni^{2+} > Co^{2+} > Zn^{2+}$.

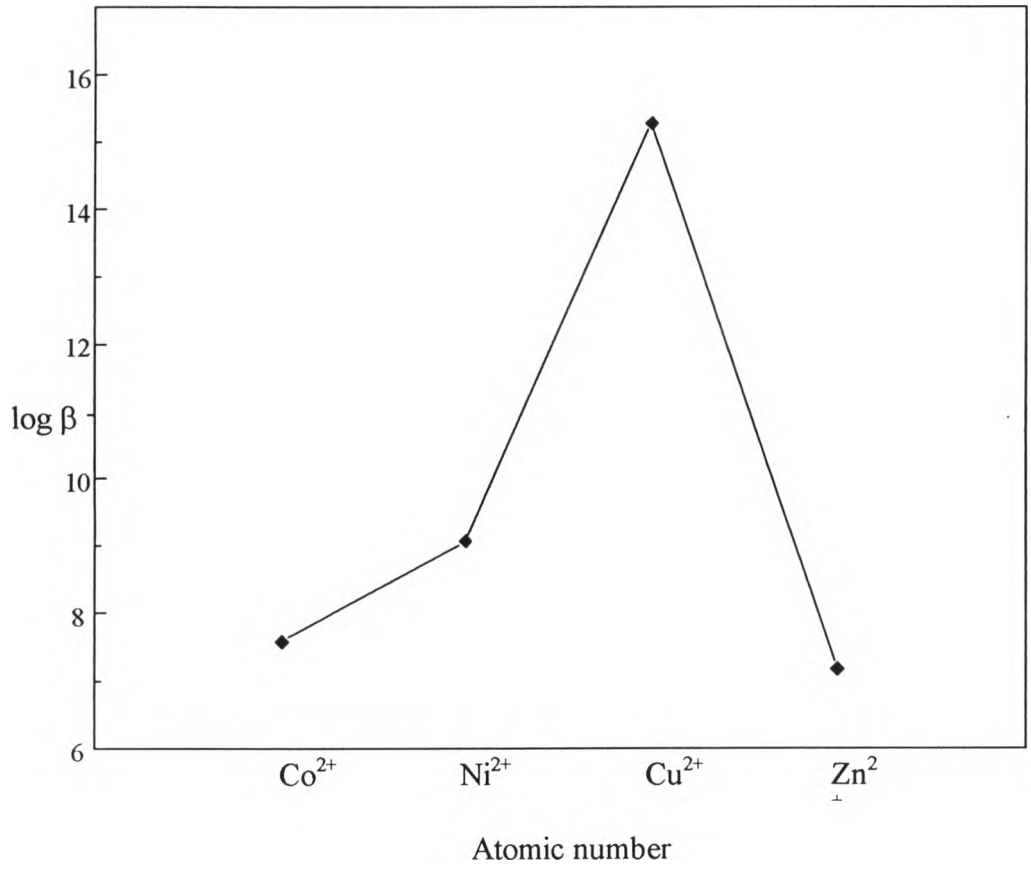

Figure 4.20 Logarithm of the stability of the transition metal with the 25,27-{2,2′-[2,2′-((2,5.8-triaza)nonyl)diphenoxy]diethyl}-*p-tert*-butylcalix[4]arene, ML^{2+} species, as the function of atomic number of the transition metal ions.